EES Catalysis

MINIREVIEW

View Article Online
View Journal | View Issue

Check for updates

Cite this: *EES Catal.*, 2024, **2**, 1228

Salt precipitation and water flooding intrinsic to electrocatalytic CO_2 reduction in acidic membrane electrode assemblies: fundamentals and remedies

Qianqian Bai,†[a] Likun Xiong,†[b] Yongjia Zhang,[a] Mutian Ma,[a] Zhenyang Jiao,[a] Fenglei Lyu, *[ac] Zhao Deng [ac] and Yang Peng *[ac]

Renewable electricity powered electrocatalytic CO_2 reduction (eCO_2R) is an emerging carbon-negative technology that upgrades CO_2 into valuable chemicals and simultaneously stores intermittent renewable energy. eCO_2R in anion exchange membrane (AEM)-based membrane electrode assemblies (MEAs) has witnessed high faradaic efficiency (FE). But severe CO_2 crossover in AEMs results in low CO_2 single-pass conversion (SPC_{CO_2}) and burdens the energy-intensive CO_2 separation process. Utilizing cation exchange membranes (CEMs) and acidic anolytes, eCO_2R in acidic MEAs is capable of addressing the CO_2 crossover issue and overcoming the SPC_{CO_2} limits in their AEM counterparts. Alkali metal cations such as K^+/Cs^+ are always adopted in acidic MEAs to suppress the competing hydrogen evolution reaction (HER) and boost eCO_2R kinetics. However, K^+/Cs^+ accumulates and precipitates in the form of carbonate/bicarbonate salts in the cathode, which accelerates water flooding, deteriorates the gas-electrode–electrolyte interface, and limits the durability of acidic eCO_2R MEAs to a few hours. In this mini-review, we discuss the fundamentals of salt precipitation and water flooding and propose potential remedies including inhibiting K^+/Cs^+ accumulation, decreasing local CO_3^{2-}/HCO_3^- concentration, and water management in gas diffusion electrodes (GDEs). We hope that this mini-review will spur more insightful solutions to address the salt precipitation and water flooding issues and push acidic eCO_2R MEAs toward industrial implementations.

Received 20th August 2024,
Accepted 3rd September 2024

DOI: 10.1039/d4ey00170b

rsc.li/eescatalysis

Open Access Article. Published on 03 settembre 2024. Downloaded on 18/12/2025 14:02:36.
This article is licensed under a Creative Commons Attribution-NonCommercial 3.0 Unported Licence.

Broader context

Electrocatalytic CO_2 reduction (eCO_2R) represents an emerging carbon-negative technology for the production of valuable chemicals from CO_2, H_2O, and renewable electricity. Benefiting from short CO_2 diffusion length ($\sim$50 nm), CO_2 electrolysis in membrane electrode assemblies (MEAs) based on gas diffusion electrodes (GDEs) greatly boosts up the current density of eCO_2R. MEAs utilizing anion exchange membranes (AEMs) have attained high eCO_2R faradaic efficiency, but suffer from severe CO_2 crossover and low carbon utilization efficiency ($\leq$50%), which burdens the energy-intensive CO_2 separation process. Utilizing cation exchange membranes (CEMs) and acidic electrolytes, acidic eCO_2R MEAs address the CO_2 crossover issue. However, alkali cations such as K^+ and Cs^+ are adopted to suppress the competing hydrogen evolution reaction (HER) and boost the eCO_2R kinetics, which causes severe salt precipitation and water flooding and seriously limits the durability of acidic MEAs to a few hours. Herein, we discuss the fundamentals of salt precipitation and water flooding in acidic eCO_2R MEAs and propose remedies that potentially overcome these issues, including mitigating/eliminating K^+/Cs^+ accumulation, reducing local CO_3^{2-}/HCO_3^- concentration, and innovating the GDE structure. This mini-review may spur more inspiration to address salt precipitation and water flooding issues in acidic eCO_2R MEAs.

1. Introduction

Electrocatalytic CO_2 reduction (eCO_2R) driven by renewable electricity from sunlight and wind holds great promise to upcycle CO_2 into valuable chemicals and simultaneously store intermittent renewable energy into chemical bonds.[1–3] In virtue of the high energy efficiency, high production rate as well as feasible scalability at the industrial scale, CO_2 electrolysis in

[a] *Soochow Institute for Energy and Material Innovations, College of Energy, Soochow University, Suzhou 215006, P. R. China. E-mail: fllv@suda.edu.cn, ypeng@suda.edu.cn*
[b] *School of Chemical and Environmental Engineering, Shanghai Institute of Technology, Shanghai, 201418, China*
[c] *Jiangsu Key Laboratory for Advanced Negative Carbon Technologies, Soochow University, Suzhou 215123, China*
† These authors contributed equally to this work.

© 2024 The Author(s). Published by the Royal Society of Chemistry

Open Access Article. Published on 03 settembre 2024. Downloaded on 18/12/2025 14:02:36.
This article is licensed under a Creative Commons Attribution-NonCommercial 3.0 Unported Licence.

zero-gap membrane electrode assemblies (MEAs) based on gas diffusion electrodes (GDEs) has drawn great attention.[4–8] Benefiting from the much shorter CO_2 diffusion length in GDEs ($\sim$50 nm) than that in conventional H-type cells ($\sim$50 μm),[9] industrially relevant current densities ($\geq$200 mA cm^{-2}) with appreciable faradaic efficiencies (>90% for CO and >80% for C_2H_4) have been attained in CO_2 MEAs utilizing anion exchange membranes (AEMs) and neutral anolytes (*e.g.* aqueous $KHCO_3$/$CsHCO_3$ solution).[10,11] However, severe CO_2 loss ($\geq$50%) brought by carbonate/bicarbonate (CO_3^{2-}/HCO_3^-) crossover in AEMs remains a significant challenge. As a result, the theoretical limits of the CO_2 single-pass conversion (SPC_{CO_2}) in AEM-based MEAs are merely 50% for CO and 25% for C_2H_4, which seriously burdens the energy-intensive CO_2 separation and purification process.[12]

Conventional CO_2 capture consumes energy from 170 to 390 kJ $mol_{CO_2}^{-1}$ depending on the CO_2 source, which translates into a voltage loss of 0.88 V caused by CO_2 recapture from the anode even with minimum energy consumption of 170 kJ mol^{-1} and 100% faradaic efficiency.[13–15] The energy penalty caused by anode CO_2 recapture for C_2H_4 is $\sim$1.55 times that of the C_2H_4 Gibbs free energy of reaction even with the maximum 25% SPC_{CO_2}, which makes the neutral MEAs untenable.[16] Though techno-economic assessments demonstrate that the industrially relevant benchmarks of SPC_{CO_2} are 30% for C_1 and 15% for C_2 products with CO_2 crossover, the same model also shows an apparent cost reduction if no CO_2 crossover exists.[17] Therefore, it is imperative to solve the CO_2 crossover issue to eliminate the energy cost for anode CO_2 recapture. It is also noteworthy that SPC_{CO_2} should not be the only target for eCO_2R MEAs. 100% SPC_{CO_2} may not be required since such high SPC_{CO_2} brings additional issues of competing HER under the low CO_2 available conditions.[16,18] Maximizing the concentration of targeted eCO_2R products in the cathode downstream, *i.e.*, maximizing SPC_{CO_2} without sacrificing the eCO_2R selectivity, is a more reasonable and practical merit.[19]

eCO_2R MEAs utilizing cation exchange membranes (CEMs) and acidic anolytes, namely acidic MEAs, are capable of addressing the CO_2 crossover issue and potentially overcoming the theoretical SPC_{CO_2} limit in neutral MEAs. In acidic MEAs, CO_3^{2-}/HCO_3^- from the cathode catalyst layer (CL) reacts with H^+ from the CEM and generates CO_2 and H_2O at the CL/CEM interface, eliminating the CO_2 crossover to the anode.[20]

In zero-gap eCO_2R MEAs, the cathode, ion exchange membrane, and anode are intimately assembled. The ion mobility of transported ionic species and ionic conductivity of the membrane dominate the ohmic loss between the cathode and anode. In acidic eCO_2R MEAs, H^+ exhibits much higher ionic mobility (3.62×10^{-7} m^2 s^{-1} V^{-1}) than CO_3^{2-} (7.46×10^{-8} m^2 s^{-1} V^{-1}) in neutral eCO_2R MEAs, rendering low ohmic loss in the ion exchange membrane and high energy efficiency.[21] More importantly, the commercially available perfluorosulfonic acid-based CEMs with high ionic conductivity and long-term stability have been widely adopted in proton exchange membrane fuel cells and water electrolyzers, which paves the way for the industrial implementation of acidic eCO_2R MEAs.

The proton source for eCO_2R in acidic MEAs is H_2O. While the proton source for the hydrogen evolution reaction (HER) is H_3O^+ under low overpotential and H_2O under high overpotential. In acidic eCO_2R MEAs with abundant H_3O^+, the Tafel step (*H + *H = H_2 + 2*) or Heyrovsky (*H + H^+ + e^- = H_2 + *) step is usually the rate-determining step for the HER with low overpotential, which shows fast kinetics with a low Tafel slope (30 mV dec^{-1} for Tafel step and 39 mV dec^{-1} for Heyrovsky step).[22] In contrast, the activation of CO_2 into $*CO_2^-$ is both kinetically sluggish with a Tafel slope of 118 mV dec^{-1}, and thermodynamically unfavorable. Moreover, the low CO_2 solubility ($\sim$34 mM) and high H_3O^+ accessibility in acidic electrolytes make the CO_2 adsorption on the surface of conventional metallic eCO_2R catalysts very difficult.[23,24] The fast kinetics of the competing HER in the H^+-rich microenvironment therefore leads to low eCO_2R selectivity in acidic MEAs.[25]

In order to suppress the HER, alkali cations such as K^+/Cs^+ are added into the acidic electrolyte, in which they play a key role in modulating the eCO_2R and HER kinetics (Fig. 1).[26] Partially desolvated alkali cations stabilize the $*CO_2^-$ intermediates *via* short range electrostatic interaction and medium range electric field-dipole interaction. The direct coordination in M^+–$O(CO_2)$ also enhances the charge transfer to the CO_2 unit.[25] Alkali cations accumulated in the outer Helmholtz plane (OHP) modify the distribution of the electric field in the double layer and suppress the migration of H_3O^+.[27] Moreover, OH^- produced during eCO_2R (eqn (1)) neutralizes the H_3O^+. Therefore, local high pH can be generated when the formation rate of OH^- compensates the migration of H_3O^+.[28] The alkali cations also play a key role in C–C bond formation. Partially desolvated alkali cations coordinate with *CO + *CO in the double layer, stabilize the key *OCCO intermediates and lower the energy barrier for C–C bond formation.[29,30] Meanwhile, alkali cations induce a hydrophobic microenvironment, which tunes the structure of interfacial water and favors the C–C coupling.[31,32]

In acidic eCO_2R MEAs, K^+/Cs^+ is usually added to the anolytes. K^+/Cs^+ is continuously dragged across the CEMs *via* the electric field and accumulates at the cathode CL, then combines with locally generated CO_3^{2-}/HCO_3^-, and forms

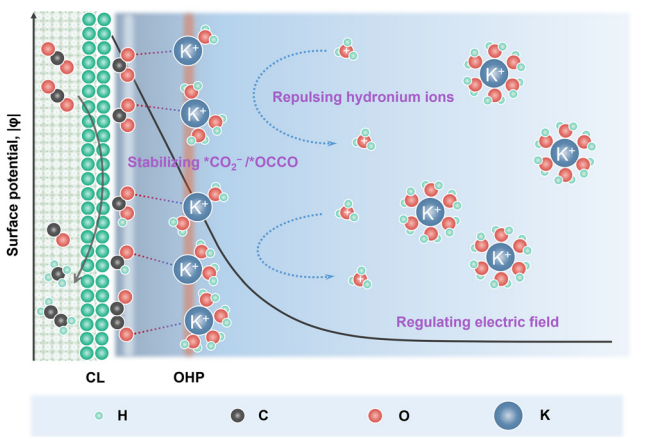

Fig. 1 Schematic illustration of the alkali cation effects in acidic eCO_2R.

Open Access Article. Published on 03 settembre 2024. Downloaded on 18/12/2025 14:02:36.
This article is licensed under a Creative Commons Attribution-NonCommercial 3.0 Unported Licence.

carbonate/bicarbonate salt precipitation. Salt precipitation destroys the hydrophobicity of GDEs and leads to severe water flooding, which not only blocks the transportation of gaseous CO_2, but also deteriorates the gas–catalyst–electrolyte interface and eventually causes MEA failure.[33]

In this mini-review, we will discuss the origins of salt precipitation and water flooding in acidic eCO_2R MEAs from a fundamental viewpoint. Then, we will summarize remedies that potentially overcome salt precipitation and water flooding issues, including mitigating/eliminating K^+/Cs^+ accumulation, reducing local CO_3^{2-}/HCO_3^- concentration, and innovating the structure of GDEs. Perspectives on how to elevate the durability, SPC_{CO_2} and energy efficiency of acidic eCO_2R MEAs through the catalyst, ionomer, membrane and their interface engineering will be discussed in the end. We hope that this mini-review will enlighten more insightful thoughts in this field and push eCO_2R in acidic MEAs toward industrial implementations.

2. Fundamentals of salt precipitation and water flooding in acidic eCO_2R MEAs

2.1. Salt precipitation in acidic eCO_2R MEAs

Alkali cations such as K^+/Cs^+ are capable of stabilizing the key $*CO_2^-$ intermediates *via* electrostatic interaction and retard the H_3O^+ diffusion kinetics through the electric field effect, thus promoting eCO_2R reactivity and suppressing the HER in acid.[25] Since CEMs are conductive to K^+/Cs^+, plenty of K^+/Cs^+ from the anolyte is continuously transported across the CEMs *via* electroosmosis and accumulates at the cathode. Owing to the generation of OH^- in eCO_2R (eqn (1)) and the suppressed H_3O^+ diffusion, the surface of cathode CL can be highly alkaline although bulk anolyte is acidic. CO_2 is chemically absorbed in the OH^--rich layer and transformed into HCO_3^- and CO_3^{2-} (eqn (2) and (3)).

$$CO_2 + H_2O + 2e^- \rightarrow CO + 2OH^- \quad (1)$$

$$CO_2 + OH^- \rightarrow HCO_3^- \quad (2)$$

$$CO_2 + 2OH^- \rightarrow CO_3^{2-} + H_2O \quad (3)$$

As shown in Fig. 2, the combination of K^+/Cs^+ and CO_3^{2-}/HCO_3^- generates K_2CO_3/Cs_2CO_3 or $KHCO_3/CsHCO_3$ salts, which precipitate in the microporous layer when their concentration exceeds the solubility limits (2.24 M for $KHCO_3$, 3.49 M for $CsHCO_3$, 7.93 M for K_2CO_3, and 8.01 M for Cs_2CO_3 at 20 °C in pure H_2O).[33] These porous and hydrophilic carbonate/bicarbonate salts accelerate electrolyte penetration into the GDEs, consequently speeding up the water flooding process. The salt precipitation strongly depends on the type and concentration of alkali cations, and the net flux of water ($J_{H_2O,net}$) in the cathode (eqn (4)). Carbonate/bicarbonate salts with higher solubility, low cation concentration in the anolyte, and low ion mobility have slower precipitation rates. Assuming that there is no crossover of anionic species such as HCO_3^-/CO_3^{2-}, the $J_{H_2O,net}$ is determined by the diffusion (J_{diff}) from the anode to the cathode driven by concentration gradients, the electro-osmotic drag (J_{eod}) caused

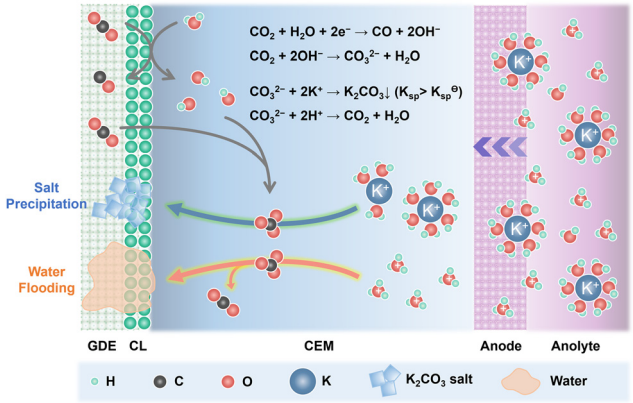

Fig. 2 Schematic illustration of the salt precipitation and water flooding process in acidic eCO_2R MEAs.

by solvated alkali cations and H_3O^+ from anode to cathode, the consumption of eCO_2R (J_{con}), and the back convection (J_{bc}) due to the repellence by the hydrophobic cathode GDE.[34]

$$J_{H_2O,net} = J_{diff} + J_{eod} - J_{con} - J_{bc} \quad (4)$$

$J_{H_2O,net}$ is dominated by the interplay of the CEM, cathode GDE, and operational current density. CEMs with low water uptake have low J_{diff} and J_{eod}. Operating at low current density and using solvated cations with low mobility decreases the J_{eod} and J_{con}. Using cathode GDEs with high hydrophobicity and CEMs with low thickness favors the J_{bc}.

2.2. Water flooding in acidic eCO_2R MEAs

Water flooding in GDEs remains a critical challenge in acidic eCO_2R MEAs since it blocks the transportation of CO_2 to the surface of catalysts and results in severe HER. Central to this issue is the gas/liquid flow scenario in porous structures. Assuming the GDE as a porous matrix with interconnected cylindrical pores (Fig. 3a–c), liquid transport in the GDE is driven by the capillary differential pressure (ΔP) between gas pressure (P_g) and liquid pressure (P_l), as shown in eqn (5) derived from the Young–Laplace equation.

$$\Delta P = P_g - P_l = \frac{2\gamma^l \cos\alpha}{r} \quad (5)$$

where γ^l is the surface tension of the liquid, α is the contact angle, and r is the pore radius.

Wetting dynamics at the interface, defined by the contact angle between the solid surface and the liquid droplets, can be categorized into the Cassie, the Cassie–Wenzel coexistence, and the Wenzel state (Fig. 3d–f). Each state delineates a unique pathway for CO_2 transportation through the GDE, corresponding to distinct flow patterns including flow-through ($\Delta P > 2\gamma^l/r$), flow-by ($-2\gamma^l/r \leq \Delta P \leq 2\gamma^l/r$), and GDE flooding ($\Delta P < -2\gamma^l/r$).

ΔP is dynamically influenced by the high H_2O flux from the anolyte to cathode GDE, which increases the P_l. In addition to H_2O diffusion from the anolyte, H_2O flux to the cathode GDE is

© 2024 The Author(s). Published by the Royal Society of Chemistry

Open Access Article. Published on 03 settembre 2024. Downloaded on 18/12/2025 14:02:36.
This article is licensed under a Creative Commons Attribution-NonCommercial 3.0 Unported Licence.

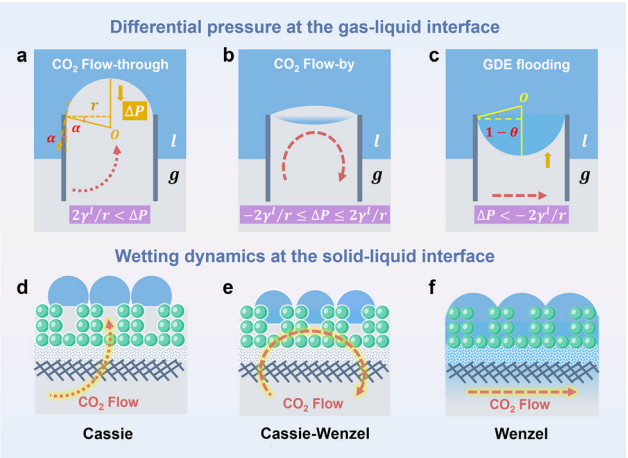

Fig. 3 Schematic illustration of differential pressure at the gas–liquid interface and corresponding (a) CO_2 flow-through, (b) CO_2 flow-by and (c) GDE flooding modes. Wetting dynamics at the solid–liquid interface including (d) Cassie state, (e) Cassie–Wenzel coexistence state, and (f) Wenzel state.

amplified *via* the electroosmosis of H^+ and K^+/Cs^+ in an acidic MEA because H^+ and K^+/Cs^+ transfer is always in conjunction with the hydrated shells, *i.e.* H_3O^+ and $K(H_2O)_m^+/Cs(H_2O)_m^+$. Additionally, excessive H_2O is generated at the CL/CEM interface during the regeneration of CO_2 from HCO_3^- and CO_3^{2-} (eqn (6) and (7)).

$$HCO_3^- + H^+ \rightarrow CO_2 + H_2O \quad (6)$$

$$CO_3^{2-} + 2H^+ \rightarrow CO_2 + H_2O \quad (7)$$

Moreover, the imbalance between CO_2 consumption and gas production rates at the interface, electrowetting, degradation of GDE hydrophobicity, and salt precipitation also contribute to the hydrostatic/hydrodynamic differential pressure by changing the P_g, γ^l and α.[35] Such variations in the pressure balance can gradually reduce ΔP below the critical transition threshold, causing the CEM system to shift from the flow-by model to the GDE flooding model. We note that the triphasic gas–electrode–electrolyte interface under operando conditions is much more complicated. For example, gases are generated at the catalyst/liquid interface due to the Joule heating. The differential pressure might vary strongly among different parts due to the complex catalyst/hydrophobic moiety/carbon interface.

3. Remedies for salt precipitation and water flooding in acidic eCO_2R MEAs

Salt precipitation and water flooding are always intertwined together, which severely deteriorates the gas–electrode–electrolyte interface and poses obstacles to the stability of acidic eCO_2R MEAs. The accumulation of K^+/Cs^+, *in situ* formation of high-concentration CO_3^{2-}/HCO_3^- on the cathode CL, and high H_2O flux from the anolyte are the main culprits for severe salt precipitation and water flooding in acidic eCO_2R MEAs. In this section, remedies including K^+/Cs^+, CO_3^{2-}/HCO_3^-, and H_2O management (Fig. 4) *via* engineering the electrodes,

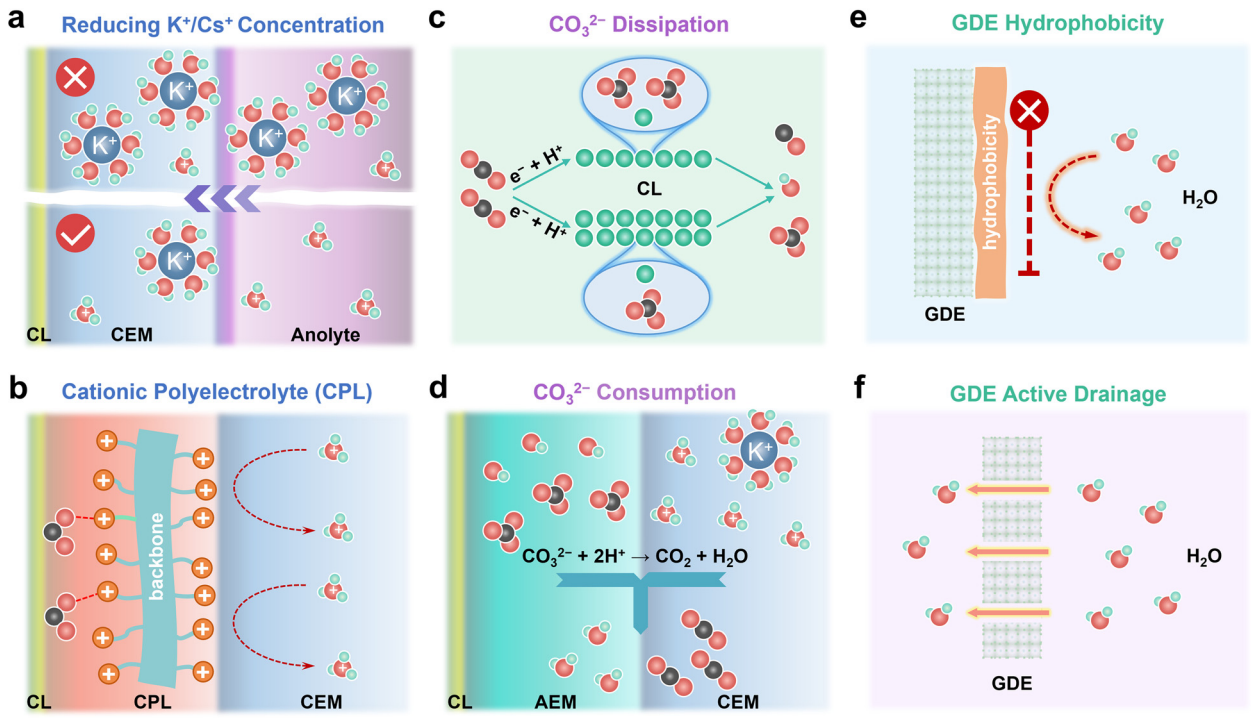

Fig. 4 Remedies of mitigating salt precipitation and water flooding in acidic eCO_2R MEAs including (a) reducing K^+/Cs^+ concentration in anolytes, (b) replacing K^+/Cs^+ with a cationic polyelectrolyte layer (CPL), (c) CO_3^{2-} dissipation in the catalyst layer (CL), (d) accelerating CO_3^{2-} consumption, (e) tailoring GDE hydrophobicity, and (f) GDE active drainage.

© 2024 The Author(s). Published by the Royal Society of Chemistry

Open Access Article. Published on 03 settembre 2024. Downloaded on 18/12/2025 14:02:36.
This article is licensed under a Creative Commons Attribution-NonCommercial 3.0 Unported Licence.

electrolyte, and membrane are proposed to mitigate these issues and enhance the durability of acidic MEAs.

3.1. Preventing K^+/Cs^+ accumulation or replacing K^+/Cs^+ with cationic polyelectrolytes

K^+/Cs^+ accumulated in the CL and microporous layer supplies cations for salt precipitation. Therefore, preventing K^+/Cs^+ accumulation represents a proactive solution to alleviate salt precipitation in acidic MEAs. Generally, the less K^+/Cs^+ migrates across the CEM, the longer the time for salts to precipitate. Reducing the concentration of K^+/Cs^+ in the anolyte is a straightforward way to limit the quantity of K^+/Cs^+ that electro-migrates from the anolyte to the cathode. In an ideal case, the concentration of K^+/Cs^+ in the anolyte should be as low as possible on the premise of high eCO_2R selectivity (Fig. 4a). By doing so, the salt precipitation kinetics are effectively decelerated. Generalized modified Poisson–Nernst–Planck (GMPNP) modeling demonstrates that the concentration of cations (C_{M^+}) and the identity of M^+ affect eCO_2R by tuning the electric field strength in the stern layer. Increasing the C_{M^+} and adding cations with smaller solvated sizes such as K^+ and Cs^+ results in higher partial current density (j_{CO}). Meanwhile, the mass transport of H^+ is inhibited when C_{M^+} is not less than C_{H^+}. Decreasing the C_{K^+} from 0.8 M to 0.02 M suppresses the $KHCO_3$ precipitation in the acidic flow cell at 200 mA cm^{-2}, but also leads to a low FE_{CO}.[36] These results match with the report from Pan *et al.*[18] In their work, the influence of Cs^+ and H^+ concentration in the anolyte on the j_{CO} and faradaic efficiency of CO (FE_{CO}) using Ag/PTFE as the cathode GDE in acidic MEAs is systematically studied. Diluted anolyte (0.01 M H_2SO_4 + 0.01 M Cs_2SO_4) is optimal for high FE_{CO} ($\sim$80%) at low current density (60 mA cm^{-2}). While low pH and Cs^+ concentration (0.2 M H_2SO_4 + 0.01 M Cs_2SO_4) are more favorable for FE_{CO} (75%) at high current density (140 mA cm^{-2}). By using 0.01 M H_2SO_4 + 0.01 M Cs_2SO_4 as anolyte, 50-hour stability at 60 mA cm^{-2} with $\sim$90% SPC_{CO_2} and 80% FE_{CO} is achieved. In a recent work, Kamiya *et al.* performed a quantitative analysis of how the transported alkali cations regulate the eCO_2R selectivity in MEAs and suggested that continuously supplying a high amount of K^+ is not necessary for C_{2+} formation.[37] Intermittently supplying concentrated $KHCO_3$ is able to extend the durability of MEAs by alleviating the salt precipitation, which provides an effective method to prevent K^+/Cs^+ accumulation.

Salt precipitation and water flooding can be mitigated but not eliminated as long as alkali cations exist in anolytes. During continuous operation in acidic MEAs, anolyte pH gradually decreases because metal cation accumulation at cathode inhibits H^+ transportation across CEMs and further induces H^+ accumulation in the anolytes. Such imbalanced ion transportation also causes the unstable operation of acidic MEAs. Operating acidic eCO_2R MEAs with pure acid or even pure water as anolytes potentially overcomes instability issues brought by imbalanced ion transportation and rapid salt precipitation. Recently, Dich *et al.* reported the using of pure water as the anolyte and periodically injecting Cs^+ containing solution into the cathode chamber to provide cations for CO_2 activation in a forward-bias bipolar membrane (f-BPM) with a porous anion exchange layer (AEL).[38] A long stability of 200 hours at 100 mA cm^{-2} with FE_{CO} $\sim$80% is achieved because cation accumulation is prohibited by using pure water as the anolyte. The use of porous AEL for recovered CO_2 recirculation in conjunction with CEMs also enables a maximum SPC_{CO2} of 52%.

Apart from using alkali cations, weakly coordinating organic cations, such as water-soluble tetraalkylammonium cations (PDDA), are intrinsically capable of supporting eCO_2R on Au and Ag on par with alkali cations.[39] Based on the modified Poisson–Boltzmann model, the electric field strength generated by the immobilized benzimidazole cationic group (CG) is in the same order as that generated by K^+,[40] which allows Cu to reach 80% C_{2+} in a pure acid electrolyte without K^+ and to operate stably for 150 h. Therefore, a cationic polyelectrolyte layer (CPL) with sufficiently high charge density sandwiched between the cathode CL and the CEM is also capable of modulating the electrical field and stabilizing $*CO_2^-$ as K^+/Cs^+ does (Fig. 4b).[41]

Polyelectrolytes with a high charge density usually have high solubility in water, which induces instability of the cathode CL/CPL/CEM interface because the water flux from the anode is increased during CO_2 recovery (eqn (6) and (7)). To mitigate the loss of polyelectrolytes, Fan *et al.* demonstrated that immobilizing poly(diallyldimethylammonium) (PDDA) on graphene oxide (GO) *via* electrostatic interaction could displace metal cations for acidic eCO_2R MEAs with pure acid or even pure water as the anolyte.[42] A 50-hour stability at 100 mA cm^{-2} with a FE_{CO} of about 70% is demonstrated in the MEA fed with 0.01 M H_2SO_4. A FE_{CO} of 78% with an energy efficiency of 30% could be achieved using a PDDA-GO modified Ag catalyst at 100 mA cm^{-2} and 40 °C.

The key role of CPLs is activating CO_2 without alkali cations, transporting CO_3^{2-} and recovered CO_2, and providing a local alkaline environment by suppressing the migration of H_3O^+. First, CPLs should have high ion exchange capacity (IEC) and maximize ionic conductivity, which favors CO_2 activation and CO_3^{2-} transportation. Second, CPLs should have moderate water uptake to manage the water content in the cathode CL since the low water uptake will cause water starvation in the cathode GDE and high water uptake will cause GDE flooding and fast H_3O^+ migration. Third, CPLs should have high mechanical and chemical stability, which not only can withstand both local acid and alkaline environments but also can mechanically stabilize the cathode CL/CPL/CEM interface. Fourth, CPLs should be permeable for gaseous CO_2, which favors transporting recovered CO_2 back to the cathode CL.

The knowledge gained from AEMs and anion exchange ionomers (AEIs) can be transferred to speed up the development of CPLs. Decent reviews on AEMs and AEIs[43–46] have summarized the desired properties, such as OH^- conductivity (60–100 mS cm^{-1}), IEC ($>$1.5 meq g^{-1}), tensile strain (20 MPa), and water uptake (50–80%), which can provide instructive knowledge for CPLs.[45] In CPLs, cationic groups such as quaternary ammonium, pyrrolidonium, piperidinium and imidazolium groups are generally integrated into the mainchain or

© 2024 The Author(s). Published by the Royal Society of Chemistry

Open Access Article. Published on 03 settembre 2024. Downloaded on 18/12/2025 14:02:36.
This article is licensed under a Creative Commons Attribution-NonCommercial 3.0 Unported Licence.

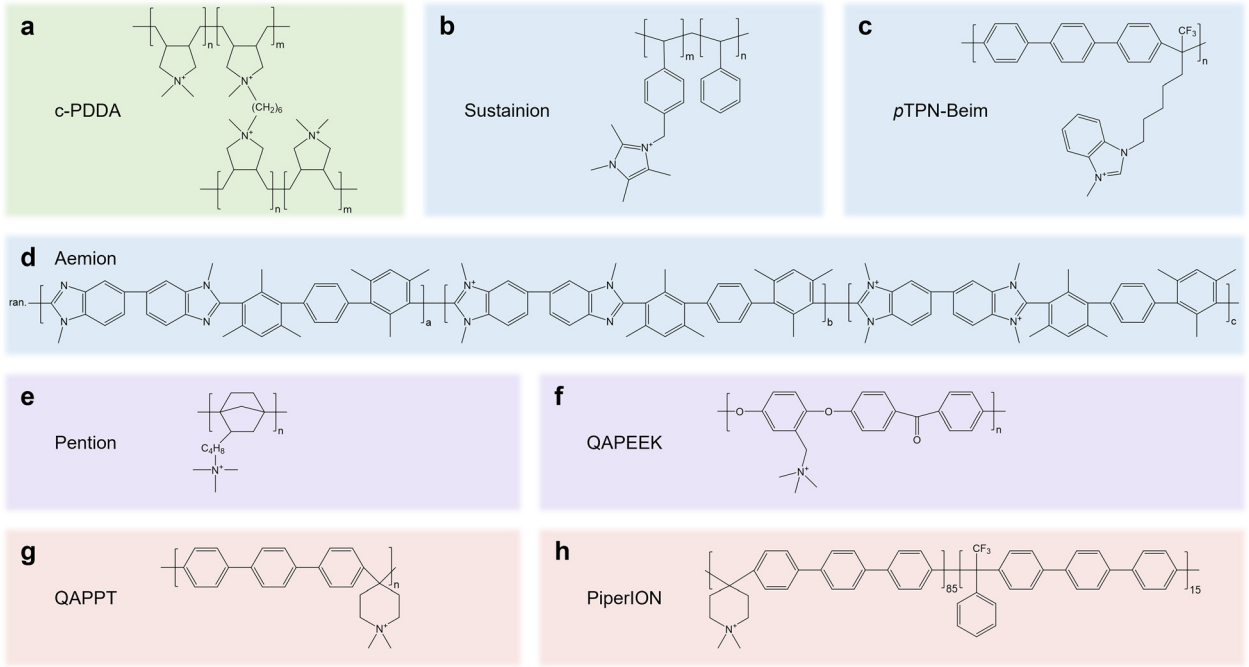

Fig. 5 Molecular structures of AEMs/AEIs that are feasible in eCO_2R electrolyzers fed with pure acid or pure water, including (a) c-PDDA, (b) Sustainion, (c) pTPN-Beim, (d) Aemion, (e) Pention, (f) QAPEEK, (g) QAPPT and (h) PiperION.

side chain of polymer backbones such as polystyrene, polybenzylimidazole, poly terphenyl, and polynorbornene. We summarize the molecular structure of AEMs/AEIs (Fig. 5) that have been proven to be feasible in pure water/pure acid-fed acidic eCO_2R electrolyzers (c-PDDA, Sustainion, Aemion, and Piperion)[16,47–49] or pure water fed neutral eCO_2R MEAs (pTPN-Beim, Pention, QAPEEK, and QAPPT),[10,50–52] which may guide the design of high-performance CPLs in the future.

3.2. Reducing local CO_3^{2-}/HCO_3^- concentration by dissipation or rapid consumption

Reducing local CO_3^{2-}/HCO_3^- concentration is also an important direction to decelerate salt precipitation kinetics since salt precipitation occurs only when the critical concentrations of metal cations and CO_3^{2-}/HCO_3^- are achieved. Dissipation and rapid consumption present promising tactics to reduce the local CO_3^{2-}/HCO_3^- concentration.

As illustrated in eqn (1)–(3), local CO_3^{2-}/HCO_3^- concentration strongly depends on the faradaic current at the cathode GDE. Increasing the amount of active site enabled by increasing the CL thickness or the density of the active site reduces the faradaic current generated per active site, thus reducing the local OH^- generated per active site (Fig. 4c).[53] In such a dissipation strategy, CO_3^{2-}/HCO_3^- is kept at low concentrations. It should be noted that CO_2 and ion transportation is slowed down when the CL is too thick. Therefore, the CL thickness should be subtly balanced. Mass-transport modelling shows that the local CO_2 concentration depends on the CL thickness, porosity and operating current densities.[9,54] Increasing the CL thickness from 1 μm to 5 μm decreases the local CO_2 concentration from 20 mM to 17 mM at 100 mA cm^{-2}. The local CO_2 concentration reduced from 17 mM to 10 mM with CL thickness of 5 μm when the current density rises from 100 mA cm^{-2} to 300 mA cm^{-2}.[55] Increasing the CL porosity enhances the gas permeability and facilitates the gas transport. Increasing the CL porosity from 0.3 to 0.7 improves the current density by more than 100 mA cm^{-2} in a wetted CL.[56]

In the electric double layer (EDL), CO_2, HCO_3^- and CO_3^{2-} are in equilibrium. According to Henry's law, increasing input CO_2 pressure (P_{CO_2}) results in increased $CO_{2(eq)}$, which tunes the $CO_{2(eq)}$–CO_3^{2-}–HCO_3^- equilibrium and potentially decreases the local CO_3^{2-}/HCO_3^- concentration. Moreover, increasing P_{CO2} is also capable of boosting the eCO_2R kinetics and suppressing the competing HER by enhancing the local CO_2 concentration.[57] When the same mole of CO_2 is fed, higher CO_2 pressure will increase the SPC_{CO_2}. However, if CO_2 availability is not the limiting factor, increasing the CO_2 pressure will not increase the SPC_{CO_2} instead.

Rapid consumption of the CO_3^{2-}/HCO_3^- generated in the CL represents another important solution to reduce the local CO_3^{2-}/HCO_3^- concentration (Fig. 4d). In a f-BPM MEA, the regeneration of CO_2 occurs at the AEM/CEM interface, where CO_3^{2-}/HCO_3^- from the AEM is consumed by H^+ from the CEM. Therefore, accelerating the transportation rate of CO_3^{2-}/HCO_3^- from the CL to the AEM/CEM interface and enlarging the AEM/CEM interface potentially increases the consumption rate of CO_3^{2-}/HCO_3^-, thereby decreasing the local CO_3^{2-}/HCO_3^- in CL. In practice, this strategy can be achieved by constructing the intimate CL/AEM/CEM interface by the catalyst-coated membrane (CCM) and direct membrane deposition (DMD) method,[58] which also has another benefit of reducing the

Open Access Article. Published on 03 settembre 2024. Downloaded on 18/12/2025 14:02:36.
This article is licensed under a Creative Commons Attribution-NonCommercial 3.0 Unported Licence.

transportation resistance of ions and increasing the overall energy efficiency.

3.3. Managing H_2O content in cathode GDEs by surface hydrophobicity and active drainage

Salt precipitation and water flooding are generally trapped into a vicious cycle and finally block the CO_2 transportation in GDEs. Though the salt precipitation problem can be potentially solved by Remedies 3.1 and 3.2, water flooding still exists because of the *in situ* formation of H_2O during CO_2 regeneration (eqn (6) and (7)). On the other hand, H_2O plays a critical role as the proton source for eCO_2R. Therefore, managing H_2O content in cathode GDEs, which can be realized by tailoring surface hydrophobicity or actively draining, is significant to balance the selectivity and stability of the acidic eCO_2R MEAs.

The cathode GDE provides spaces for uniformly distributing CO_2, H_2O, and electrons. However, the transport pathways for CO_2 and H_2O are usually intertwined, which impedes CO_2 diffusion. Hydrophobic treatment of the GDE is therefore essential to decouple CO_2 and H_2O transportation (Fig. 4e). In previous work, Wang *et al.* reported a hydrophobized integral GDE embedding undercoordinated Ni–N–C active sites (NiNF) for full-pH CO_2 electroreduction in MEAs.[59] By virtue of the integral architecture, hierarchical porosity, and high hydrophobicity, it not only enhances CO_2 transportation but also mitigates salt precipitation and water flooding. NiNF exhibits a near-unity faradaic efficiency of CO and stable operation for more than 273 hours in neutral MEAs and a high single-pass CO_2 conversion of 78% in acidic MEAs. Post-mortem characterizations reveal that the failure of MEAs is mainly attributed to the loss of hydrophobicity.

Conventional GDEs are composed of macroporous carbon fiber paper (CFP), microporous layer (MPL), and CL, among which micropores in the MPL are the most easily flooded due to electrochemical wetting by water. Active draining by innovating the GDE structure holds promise to enhance its tolerance to water flooding and extend its durability (Fig. 4f). For example, through tailoring the wettability gradient and introducing large-size pores by laser drilling in a Janus carbon-based GDE, water spontaneously transports from the hydrophobic side to hydrophilic side, enabling a remarkable antiflooding capability.[60] In addition to conventional carbon-based GDEs, metal foam-based GDEs have recently drawn great attention because of the high conductivity of the metal foam and abundant large pores with microns in size. A hydrophobic catalytic layer can be *in situ* grown on metal foams through etching metal foams or electrodeposition.[11,61] Such architecture not only enables a high CO_2 diffusion rate by surface hydrophobicity but also enhances resilience to flooding because the large pores are favorable for drainage, offering great opportunities to mitigate GDE flooding.

In Remedy 3.1, reducing the concentration of K^+/Cs^+ helps to extend the stability of acidic MEAs and simultaneously utilizes the cation effect to keep the high eCO_2R selectivity. However, the salt precipitation after long-term operation is unavoidable since the CEMs are permeable to K^+/Cs^+. Utilizing a CPL to replace K^+/Cs^+ can eliminate the salt precipitation issue. But how to rationally fabricate the CPL with high chemical and mechanical robustness, and stabilize the cathode CL/CPL/CEM interface still remains to be explored. In Remedy 3.2, increasing the CL thickness or the density of active sites can reduce the local concentration of CO_3^{2-}, but will cause the problem of slow CO_2 and ion transfer. Constructing an intimate cathode CL/AEM/CEM interface by the CCM or DMD method can boost the CO_3^{2-} transfer and consumption, and increase the energy efficiency at the same time. The flux of H^+, CO_3^{2-}, and CO_2 should be carefully balanced at the CL/AEM/CEM interface. In Remedy 3.3, increasing the hydrophobicity of GDEs can facilitate CO_2 transportation and increase the resistance to water flooding. But the loss of hydrophobicity by electrowetting and loss of PTFE binder over time cannot be avoided. The active drainage of GDEs can effectively manage water content in GDEs. More efforts should be devoted to properly engineering the distribution of wettable areas since the flooding behavior and water distribution in cathode GDEs remain elusive, which may increase the fabrication of the GDEs. In addition, periodically adding cations or refreshing the anode electrolyte is necessary to compensate for the loss of cations brought by the water flow out of the electrolyte.

We note that some of these strategies including reducing the concentration of K^+/Cs^+, tailoring the porosity and thickness of cathode CL, constructing a cathode CL/membrane interface for favorable ion transfer, increasing the hydrophobicity or constructing wettable area for water management in the cathode GDE can be extended to the neutral/alkaline eCO_2R MEA too. But the optimal conditions in these strategies vary since neutral/alkaline eCO_2R MEAs manifest different local environments (such as local CO_2 concentration and local pH) from acidic MEAs. The AEIs of neutral/alkaline eCO_2R are critical for managing the CO_2 gas and CO_3^{2-} ion transfer in the cathode CL. But the CPLs in acidic eCO_2R MEAs should be more challenging since they not only provide the gas and ion transfer pathway but also are capable of stabilizing the cathode CL/CPL/CEM interface during CO_2 recovery.

4. Summary and perspective

Acidic MEAs have become an important direction in the development of eCO_2R for industrial applications because of their high carbon utilization and energy efficiency. However, the durability issue of acidic eCO_2R MEAs brought by salt precipitation and water flooding remains challenging. In this minireview, we discuss the origins of salt precipitation and water flooding from the fundamental viewpoint and propose potential remedies including inhibiting K^+/Cs^+ accumulation, decreasing local CO_3^{2-}/HCO_3^-, and water management in GDEs.

Apart from the electrode, electrolyte, and membrane engineering, recovery steps/washing is necessary to recover the performance loss caused by salt precipitation and water flooding with relatively low operation cost. For example, washing the cathode GDE with water can dissolve the salt precipitates and

© 2024 The Author(s). Published by the Royal Society of Chemistry

Open Access Article. Published on 03 settembre 2024. Downloaded on 18/12/2025 14:02:36.
This article is licensed under a Creative Commons Attribution-NonCommercial 3.0 Unported Licence.

maintain the moderate FE_{CO} (85%) during continuous electrolysis.[62] Periodically activating and regenerating the cathode GDE with cation containing solution (1 M CsOH in 1 : 3 isopropanol/water mixture) in the pure water-fed electrolyzer can maintain the stability for 200 h.[38,63] In addition to the commonly used aqueous electrolyte, organic electrolyte can also be utilized to reduce the carbonation of aqueous electrolyte. By utilizing dimethyl sulfoxide as the solvent and acetic acid/acetate as the proton source in the aprotic solvent-based eCO_2R system, Chu *et al.* demonstrated that attenuating the water content in an organic medium and using a nonnucleophilic buffer with a matched pKa simultaneously mitigates carbonation and the HER.[64]

Although progress has been made to address the salt precipitation and water flooding to extend the durability of acidic eCO_2R MEAs, there is still a long way ahead to meet the requirements for stability (5 years), energy efficiency ($\sim$50%), and SPC_{CO2} (30% and 15% for C_1 and C_2 products) according to the techno-economic assessment.[17] To push acidic eCO_2R MEAs toward large-scale implementation, research efforts also should be devoted to the following fields:

(1) Fabricating selective and stable eCO_2R electrocatalysts for acidic MEAs. Some heterogeneous molecular electrocatalysts are intrinsically active and selective for acidic eCO_2R in a pure water-fed BPM electrolyzer, which completely eliminates the salt precipitation issue. For example, the acid-tolerant $[Ni(1,4,8,11\text{-tetraazacyclotetradecane})]^{2+}$ catalyst achieves >30% CO selectivity at 100 mA cm^{-2} in a zero-gap r-BPM device fed with pure water and CO_2.[65] Cobalt phthalocyanine (CoPc) achieved 53% CO selectivity at 100 mA cm^{-2} and an SPC up to 51%.[66] Cobalt tetraaminophthalocyanine covalently anchored on the positively charged polyfluorene backbone (PF-CoTAPc) achieves 82.6% FE_{CO} at 100 mA cm^{-2} and 87.8% CO_2 utilization.[67] More efforts are needed to develop electrocatalysts with intrinsically high eCO_2R selectivity and stability in pure acid or water.

Nanostructured electrocatalysts have the benefit of reducing the current/area and modulating the concentration of reactants/intermediates/products. But the coexistence of H^+, adsorbates such as *CO and negative bias in acidic eCO_2R MEAs generates highly corrosive conditions for the popular M–N–C, Cu and Ag based electrocatalysts, causing demetallation in M–N–C and migration of surface-active metal atoms, and deactivating these electrocatalysts.[68,69] We think the activity, selectivity, stability, and cost of the nanostructured electrocatalysts should all be taken into account and well-balanced. Constructing highly stable electrocatalysts, which are resilient to harsh conditions through strong metal–support interactions or surface polymer/carbon coating, may be able to alleviate the corrosion of electrocatalysts in acidic MEAs.

(2) Designing highly conductive and stable CPLs. CPLs play crucial roles in manipulating the CO_2, H_2O, CO_3^{2-}/HCO_3^- and K^+/Cs^+ transportation in the triphasic gas–electrode–electrolyte interface.[46] CPLs with high ionic conductivity and microphase separation structure are expected to decouple the CO_2 and ion transfer pathway and boost the eCO_2R kinetics.[45] Moreover, more chemically and mechanically stable CPLs are highly desired to enhance the durability of acidic MEAs.

(3) Systematically engineering the cathode CL/membrane interface. For the conventional catalyst-coated substrate (CCS) method, the cathode CL/membrane ionic interface contributes the major voltage loss,[70] which hinders the energy efficiency and current density. Constructing novel micro-/nano-structures such as three-dimensional (3D) ordered CLs with interlocked catalyst/membrane interface should boost the ion transfer and elevate the energy efficiency.[71]

(4) Quantitatively understanding and optimizing acidic eCO_2R MEAs by numerical simulations. In contrast to the conventional try-and-error experimental approach, numerical simulations play a key role in the development of eCO_2R electrolyzers by providing a deep and quantitative understanding of the transportation behavior of reactants/intermediates/products and their local concentration at the electrode/electrolyte interface with less cost.[72–77] The insight gained from numerical simulation will provide useful guidance for developing selective and stable acidic eCO_2R MEAs.

(5) Operando characterizations and monitoring the chemical microenvironment and interface in acidic eCO_2R MEAs. Monitoring the chemical microenvironment and the interface during operando conditions is significant for unraveling the failure mechanism of acidic eCO_2R MEAs, but is still at the early stage. Developing more *in situ* and operando techniques such as synchrotron radiation X-ray absorption spectroscopy (XAS), Raman spectroscopy, operando X-ray diffraction (XRD), and electrochemical impedance spectroscopy (EIS) with distribution of relaxation times (DRT) analysis is highly suggested to reveal the electronic structure of catalysts, evolution of the intermediates and local pH, salt precipitation and water flooding in GDEs, and changes in the catalyst/membrane interface.[78–81]

Author contributions

Q. B., L. X., Y. Z., M. M. and Z. J.: writing – original draft and editing, investigation, visualization, data curation. Y. P., Z. D. and F. L.: conceptualization, resources, supervision, methodology, writing – review and editing, funding acquisition.

Data availability

No primary research results, software or code have been included and no new data were generated or analysed as part of this review.

Conflicts of interest

There are no conflicts to declare.

Open Access Article. Published on 03 settembre 2024. Downloaded on 18/12/2025 14:02:36.
This article is licensed under a Creative Commons Attribution-NonCommercial 3.0 Unported Licence.

Acknowledgements

This work is supported by the National Natural Science Foundation of China (No. 22309125, 22072101, 22075193, 22109099), the Natural Science Foundation of Jiangsu Province (No. BK20220483, BK20211306, BK20220027, BK20221239), the Natural Science Foundation of the Jiangsu Higher Education Institutions of China (22KJB150010), Six Talent Peaks Project in Jiangsu Province (No. TD-XCL-006), Chen Guang project from Shanghai Municipal Education Commission and Shanghai Education Development Foundation, and the Priority Academic Program Development (PAPD) of Jiangsu Higher Education Institutions.

Notes and references

1 S. M. Jordaan and C. Wang, *Nat. Catal.*, 2021, **4**, 915–920.
2 C. Chen, H. Jin, P. Wang, X. Sun, M. Jaroniec, Y. Zheng and S.-Z. Qiao, *Chem. Soc. Rev.*, 2024, **53**, 2022–2055.
3 C. Tang, Y. Zheng, M. Jaroniec and S.-Z. Qiao, *Angew. Chem., Int. Ed.*, 2021, **60**, 19572–19590.
4 Z. Zhang, X. Huang, Z. Chen, J. Zhu, B. Endrődi, C. Janáky and D. Deng, *Angew. Chem., Int. Ed.*, 2023, **62**, e202302789.
5 C. Yan, D. Gao, J.-J. Velasco-Vélez and G. Wang, *EES Catal.*, 2024, **2**, 220–230.
6 C. A. Giron Rodriguez, N. C. Kani, A. B. Moss, B. O. Joensen, S. Garg, W. Deng, T. Wilson, J. R. Varcoe, I. Chorkendorff and B. Seger, *EES Catal.*, 2024, **2**, 850–861.
7 E. F. Johnson, E. Boutin, S. Liu and S. Haussener, *EES Catal.*, 2023, **1**, 704–719.
8 S. Kwon, T.-H. Kong, N. Park, P. Thangavel, H. Lee, S. Shin, J. Cha and Y. Kwon, *EES Catal.*, 2024, **2**, 911–922.
9 T. Burdyny and W. A. Smith, *Energy Environ. Sci.*, 2019, **12**, 1442–1453.
10 Z. Yin, H. Peng, X. Wei, H. Zhou, J. Gong, M. Huai, L. Xiao, G. Wang, J. Lu and L. Zhuang, *Energy Environ. Sci.*, 2019, **12**, 2455–2462.
11 J. Han, B. Tu, P. An, J. Zhang, Z. Yan, X. Zhang, C. Long, Y. Zhu, Y. Yuan, X. Qiu, Z. Yang, X. Huang, S. Yan and Z. Tang, *Adv. Mater.*, 2024, e2313926.
12 J. A. Rabinowitz and M. W. Kanan, *Nat. Commun.*, 2020, **11**, 5231.
13 J. E. Huang, F. Li, A. Ozden, A. S. Rasouli, F. P. G. D. Arquer, S. Liu, S. Zhang, M. Luo, X. Wang, Y. Lum, Y. Xu, K. Bertens, R. K. Miao, C.-T. Dinh, D. Sinton and E. H. Sargent, *Science*, 2021, **372**, 1074–1078.
14 N. McQueen, K. V. Gomes, C. McCormick, K. Blumanthal, M. Pisciotta and J. Wilcox, *Prog. Energy*, 2021, **3**, 032001.
15 K. V. Petrov, C. I. Koopman, S. Subramanian, M. T. M. Koper, T. Burdyny and D. A. Vermaas, *Nat. Energy*, 2024, **9**, 932–938.
16 C. P. O'Brien, R. K. Miao, S. Liu, Y. Xu, G. Lee, A. Robb, J. E. Huang, K. Xie, K. Bertens, C. M. Gabardo, J. P. Edwards, C.-T. Dinh, E. H. Sargent and D. Sinton, *ACS Energy Lett.*, 2021, **6**, 2952–2959.
17 H. Shin, K. U. Hansen and F. Jiao, *Nat. Sustainability*, 2021, **4**, 911–919.
18 B. Pan, J. Fan, J. Zhang, Y. Luo, C. Shen, C. Wang, Y. Wang and Y. Li, *ACS Energy Lett.*, 2022, **7**, 4224–4231.
19 S. C. da Cunha and J. Resasco, *Nat. Commun.*, 2023, **14**, 5513.
20 A. Ozden, F. P. García de Arquer, J. E. Huang, J. Wicks, J. Sisler, R. K. Miao, C. P. O'Brien, G. Lee, X. Wang, A. H. Ip, E. H. Sargent and D. Sinton, *Nat. Sustainability*, 2022, **5**, 563–573.
21 J. R. Varcoe, P. Atanassov, D. R. Dekel, A. M. Herring, M. A. Hickner, P. A. Kohl, A. R. Kucernak, W. E. Mustain, K. Nijmeijer, K. Scott, T. Xu and L. Zhuang, *Energy Environ. Sci.*, 2014, **7**, 3135–3191.
22 X. Tian, P. Zhao and W. Sheng, *Adv. Mater.*, 2019, **31**, 1808066.
23 Y. Y. Birdja, E. Pérez-Gallent, M. C. Figueiredo, A. J. Göttle, F. Calle-Vallejo and M. T. M. Koper, *Nat. Energy*, 2019, **4**, 732–745.
24 S. Feng, X. Wang, D. Cheng, Y. Luo, M. Shen, J. Wang, W. Zhao, S. Fang, H. Zheng, L. Ji, X. Zhang, W. Xu, Y. Liang, P. Sautet and J. Zhu, *Angew. Chem., Int. Ed.*, 2024, **63**, e202317942.
25 M. C. O. Monteiro, F. Dattila, B. Hagedoorn, R. García-Muelas, N. López and M. T. M. Koper, *Nat. Catal.*, 2021, **4**, 654–662.
26 Y. Dong, M. Ma, Z. Jiao, S. Han, L. Xiong, Z. Deng and Y. Peng, *Chin. Chem. Lett.*, 2024, **35**, 109049.
27 J. Gu, S. Liu, W. Ni, W. Ren, S. Haussener and X. Hu, *Nat. Catal.*, 2022, **5**, 268–276.
28 C. J. Bondue, M. Graf, A. Goyal and M. T. M. Koper, *J. Am. Chem. Soc.*, 2021, **143**, 279–285.
29 S.-J. Shin, H. Choi, S. Ringe, D. H. Won, H.-S. Oh, D. H. Kim, T. Lee, D.-H. Nam, H. Kim and C. H. Choi, *Nat. Commun.*, 2022, **13**, 5482.
30 Z. Zhang, H. Li, Y. Shao, L. Gan, F. Kang, W. Duan, H. A. Hansen and J. Li, *Nat. Commun.*, 2024, **15**, 612.
31 G. P. Heim, M. A. Bruening, C. B. Musgrave, W. A. Goddard, J. C. Peters and T. Agapie, *Joule*, 2024, **8**, 1312–1321.
32 X. Yang, H. Ding, S. Li, S. Zheng, J.-F. Li and F. Pan, *J. Am. Chem. Soc.*, 2024, **146**, 5532–5542.
33 M. Sassenburg, M. Kelly, S. Subramanian, W. A. Smith and T. Burdyny, *ACS Energy Lett.*, 2023, **8**, 321–331.
34 A. Reyes, R. P. Jansonius, B. A. W. Mowbray, Y. Cao, D. G. Wheeler, J. Chau, D. J. Dvorak and C. P. Berlinguette, *ACS Energy Lett.*, 2020, **5**, 1612–1618.
35 D. Wakerley, S. Lamaison, J. Wicks, A. Clemens, J. Feaster, D. Corral, S. A. Jaffer, A. Sarkar, M. Fontecave, E. B. Duoss, S. Baker, E. H. Sargent, T. F. Jaramillo and C. Hahn, *Nat. Energy*, 2022, **7**, 130–143.
36 H.-G. Qin, F.-Z. Li, Y.-F. Du, L.-F. Yang, H. Wang, Y.-Y. Bai, M. Lin and J. Gu, *ACS Catal.*, 2023, **13**, 916–926.
37 S. Kato, S. Ito, S. Nakahata, R. Kurihara, T. Harada, S. Nakanishi and K. Kamiya, *ChemSusChem*, 2024, e202401013.
38 J. Disch, S. Ingenhoven and S. Vierrath, *Adv. Energy Mater.*, 2023, **13**, 2301614.

© 2024 The Author(s). Published by the Royal Society of Chemistry

Open Access Article. Published on 03 settembre 2024. Downloaded on 18/12/2025 14:02:36.
This article is licensed under a Creative Commons Attribution-NonCommercial 3.0 Unported Licence.

39 S. Weng, W. L. Toh and Y. Surendranath, *J. Am. Chem. Soc.*, 2023, **145**, 16787–16795.
40 M. Fan, J. E. Huang, R. K. Miao, Y. Mao, P. Ou, F. Li, X.-Y. Li, Y. Cao, Z. Zhang, J. Zhang, Y. Yan, A. Ozden, W. Ni, Y. Wang, Y. Zhao, Z. Chen, B. Khatir, C. P. O'Brien, Y. Xu, Y. C. Xiao, G. I. N. Waterhouse, K. Golovin, Z. Wang, E. H. Sargent and D. Sinton, *Nat. Catal.*, 2023, **6**, 763–772.
41 D. Song, Y. Lian, M. Wang, Y. Su, F. Lyu, Z. Deng and Y. Peng, *eScience*, 2023, **3**, 100097.
42 J. Fan, B. Pan, J. Wu, C. Shao, Z. Wen, Y. Yan, Y. Wang and Y. Li, *Angew. Chem., Int. Ed.*, 2024, **63**, e202317828.
43 S. Favero, I. E. L. Stephens and M.-M. Titirci, *Adv. Mater.*, 2024, **36**, 2308238.
44 S. Garg, C. A. Giron Rodriguez, T. E. Rufford, J. R. Varcoe and B. Seger, *Energy Environ. Sci.*, 2022, **15**, 4440–4469.
45 D. A. Salvatore, C. M. Gabardo, A. Reyes, C. P. O'Brien, S. Holdcroft, P. Pintauro, B. Bahar, M. Hickner, C. Bae, D. Sinton, E. H. Sargent and C. P. Berlinguette, *Nat. Energy*, 2021, **6**, 339–348.
46 E. W. Lees, B. A. W. Mowbray, F. G. L. Parlane and C. P. Berlinguette, *Nat. Rev. Mater.*, 2022, **7**, 55–64.
47 H.-G. Qin, Y.-F. Du, Y.-Y. Bai, F.-Z. Li, X. Yue, H. Wang, J.-Z. Peng and J. Gu, *Nat. Commun.*, 2023, **14**, 5640.
48 X. She, L. Zhai, Y. Wang, P. Xiong, M. M.-J. Li, T.-S. Wu, M. C. Wong, X. Guo, Z. Xu, H. Li, H. Xu, Y. Zhu, S. C. E. Tsang and S. P. Lau, *Nat. Energy*, 2024, **9**, 81–91.
49 M. Heßelmann, J. K. Lee, S. Chae, A. Tricker, R. G. Keller, M. Wessling, J. Su, D. Kushner, A. Z. Weber and X. Peng, *ACS Appl. Mater. Interfaces*, 2024, **16**, 24649–24659.
50 L. Xue, Z. Gao, T. Ning, W. Li, J. Li, J. Yin, L. Xiao, G. Wang and L. Zhuang, *Angew. Chem., Int. Ed.*, 2023, **62**, e202309519.
51 M. Zhuansun, Y. Liu, R. Lu, F. Zeng, Z. Xu, Y. Wang, Y. Yang, Z. Wang, G. Zheng and Y. Wang, *Angew. Chem., Int. Ed.*, 2023, **62**, e202309875.
52 W. Li, Z. Yin, Z. Gao, G. Wang, Z. Li, F. Wei, X. Wei, H. Peng, X. Hu, L. Xiao, J. Lu and L. Zhuang, *Nat. Energy*, 2022, **7**, 835–843.
53 Q. Xu, A. Xu, S. Garg, A. B. Moss, I. Chorkendorff, T. Bligaard and B. Seger, *Angew. Chem., Int. Ed.*, 2023, **62**, e202214383.
54 J. C. Bui, E. W. Lees, L. M. Pant, I. V. Zenyuk, A. T. Bell and A. Z. Weber, *Chem. Rev.*, 2022, **122**, 11022–11084.
55 Y. C. Tan, K. B. Lee, H. Song and J. Oh, *Joule*, 2020, **4**, 1104–1120.
56 L.-C. Weng, A. T. Bell and A. Z. Weber, *Phys. Chem. Chem. Phys.*, 2018, **20**, 16973–16984.
57 H. Li, H. Li, P. Wei, Y. Wang, Y. Zang, D. Gao, G. Wang and X. Bao, *Energy Environ. Sci.*, 2023, **16**, 1502–1510.
58 T. Alkayyali, A. S. Zeraati, H. Mar, F. Arabyarmohammadi, S. Saber, R. K. Miao, C. P. O'Brien, H. Liu, Z. Xie, G. Wang, E. H. Sargent, N. Zhao and D. Sinton, *ACS Energy Lett.*, 2023, **8**, 4674–4683.
59 M. Wang, L. Lin, Z. Zheng, Z. Jiao, W. Hua, G. Wang, X. Ke, Y. Lian, F. Lyu, J. Zhong, Z. Deng and Y. Peng, *Energy Environ. Sci.*, 2023, **16**, 4423–4431.
60 Q. Wen, S. Pan, Y. Li, C. Bai, M. Shen, H. Jin, F. Ning, X. Fu and X. Zhou, *ACS Energy Lett.*, 2022, **7**, 3900–3909.
61 M. Sun, J. Cheng and M. Yamauchi, *Nat. Commun.*, 2024, **15**, 491.
62 B. Endrődi, E. Kecsenovity, A. Samu, F. Darvas, R. V. Jones, V. Török, A. Danyi and C. Janáky, *ACS Energy Lett.*, 2019, **4**, 1770–1777.
63 B. Endrődi, A. Samu, E. Kecsenovity, T. Halmágyi, D. Sebők and C. Janáky, *Nat. Energy*, 2021, **6**, 439–448.
64 A. T. Chu, O. Jung, W. L. Toh and Y. Surendranath, *J. Am. Chem. Soc.*, 2023, **145**, 9617–9623.
65 B. Siritanaratkul, M. Förster, F. Greenwell, P. K. Sharma, E. H. Yu and A. J. Cowan, *J. Am. Chem. Soc.*, 2022, **144**, 7551–7556.
66 B. Siritanaratkul, P. K. Sharma, E. H. Yu and A. J. Cowan, *Adv. Mater. Interfaces*, 2023, **10**, 2300203.
67 G. Li, L. Huang, C. Wei, H. Shen, Y. Liu, Q. Zhang, J. Su, Y. Song, W. Guo, X. Cao, B. Z. Tang, M. Robert and R. Ye, *Angew. Chem., Int. Ed.*, 2024, **63**, e202400414.
68 Y. Yang, S. Louisia, S. Yu, J. Jin, I. Roh, C. Chen, M. V. Fonseca Guzman, J. Feijóo, P.-C. Chen, H. Wang, C. J. Pollock, X. Huang, Y.-T. Shao, C. Wang, D. A. Muller, H. D. Abruña and P. Yang, *Nature*, 2023, **614**, 262–269.
69 X. Li, P. Zhang, L. Zhang, G. Zhang, H. Gao, Z. Pang, J. Yu, C. Pei, T. Wang and J. Gong, *Chem. Sci.*, 2023, **14**, 5602–5607.
70 K. U. Hansen, L. H. Cherniack and F. Jiao, *ACS Energy Lett.*, 2022, **7**, 4504–4511.
71 L. Wan, J. Liu, D. Lin, Z. Xu, Y. Zhen, M. Pang, Q. Xu and B. Wang, *Energy Environ. Sci.*, 2024, **17**, 3396–3408.
72 L.-C. Weng, A. T. Bell and A. Z. Weber, *Energy Environ. Sci.*, 2019, **12**, 1950–1968.
73 L.-C. Weng, A. T. Bell and A. Z. Weber, *Energy Environ. Sci.*, 2020, **13**, 3592–3606.
74 N. Gupta, M. Gattrell and B. MacDougall, *J. Appl. Electrochem.*, 2006, **36**, 161–172.
75 Y. Lum, B. Yue, P. Lobaccaro, A. T. Bell and J. W. Ager, *J. Phys. Chem. C*, 2017, **121**, 14191–14203.
76 Y. Xie, P. Ou, X. Wang, Z. Xu, Y. C. Li, Z. Wang, J. E. Huang, J. Wicks, C. McCallum, N. Wang, Y. Wang, T. Chen, B. T. W. Lo, D. Sinton, J. C. Yu, Y. Wang and E. H. Sargent, *Nat. Catal.*, 2022, **5**, 564–570.
77 C.-T. Dinh, T. Burdyny, M. G. Kibria, A. Seifitokaldani, C. M. Gabardo, F. P. G. D. Arquer, A. Kiani, J. P. Edwards, P. D. Luna, O. S. Bushuyev, C. Zou, R. Quintero-Bermudez, Y. Pang, D. Sinton and E. H. Sargent, *Science*, 2018, **360**, 783–787.
78 S. Brückner, Q. Feng, W. Ju, D. Galliani, A. Testolin, M. Klingenhof, S. Ott and P. Strasser, *Nat. Chem. Eng.*, 2024, **1**, 229–239.
79 B. O. Joensen, J. A. Zamora Zeledon, L. Trotochaud, A. Sartori, M. Mirolo, A. B. Moss, S. Garg, I. Chorkendorff, J. Drnec, B. Seger and Q. Xu, *Joule*, 2024, **8**, 1754–1771.
80 A. B. Moss, S. Garg, M. Mirolo, C. A. Giron Rodriguez, R. Ilvonen, I. Chorkendorff, J. Drnec and B. Seger, *Joule*, 2023, **7**, 350–365.
81 Y. Qu, K. Yang, W. Li, G. Wang, L. Xiao, G. Wang and L. Zhuang, *ACS Energy Lett.*, 2024, **9**, 3042–3048.

© 2024 The Author(s). Published by the Royal Society of Chemistry